A Comprehensive Analysis of the Absorption Spectrum of Conducting Ferromagnetic Wires

Iñigo Liberal, Iñigo Ederra, Cristina Gómez-Polo, Alberto Labrador, Jose Ignacio Pérez-Landazábal and Ramón Gonzalo, *Member, IEEE*

***Abstract*—A detailed analysis of the absorption spectrum of conductive ferromagnetic wires is presented. The absorption spectrum is computed from the solution to the scattering problem, and circuit models are formulated to clarify the interplay between losses, skin-effect and wire geometry. Both infinitely-long wires and the axial resonances introduced by finite-length wires are considered. The theoretical results are validated experimentally through measurements within a metallic rectangular waveguide.**

***Index Terms*—Ferromagnetic wires, Absorption Spectrum, Ferromagnetic Resonance**

I. Introduction

An accurate knowledge of the absorption spectrum of ferromagnetic wires is required from both a technological and a material science point of view. On the one hand, not only is the absorption spectrum fundamental to the design of electromagnetic absorbers [1]–[3], but it is also a key aspect for the development of many other wire-based systems, such as self-sensing materials [4], [5], transmission control screens [6], [7] and artificial electromagnetic materials [8]–[12]. On the other hand, the absorption spectrum of ferromagnetic wires is employed to determine the ferromagnetic resonance (FMR) frequency, and thus investigate the magnetic properties of the wires. To this end, the absorption spectrum is typically measured in resonant cavities [13]–[15] microstrip lines [16] and/or coaxial lines [17]–[19].

Despite all this interest, the absorption spectrum of conductive ferromagnetic wires is not always well-understood. As a matter of fact, its interpretation is not straightforward due to the inter-coupling between losses, skin-effect and wire geometry. For example, although losses are maximal at the FMR, in general this does not imply a peak of absorption [14]. Therefore, the FMR does not necessarily enhance the absorption in the wires and it cannot be easily identified. In addition, axial resonances can be excited in finite-length wires, introducing additional complexity to the absorption spectrum.

Previous works have solved the scattering problem of infinitely-long ferromagnetic wires [13], [20], [21], while the antenna approximation has been applied to find the electromagnetic response of finite-length wires [9]. Whereas these works have provided the necessary tools to estimate the absorption spectrum of the wires, this contribution presents a comprehensive analysis of the absorption spectrum of conductive ferromagnetic wires, clarifying the aforementioned issues. The analysis is thus intended to enable an intuitive interpretation of the absorption spectrum, and to simplify the design of wire-based systems. To this end, the absorption spectrum is determined from the solution to the scattering problem, and circuit models are formulated to provide more physical insight into the absorption and scattering phenomena. Finally, the theoretical results are experimentally validated with measurements within a metallic rectangular waveguide.

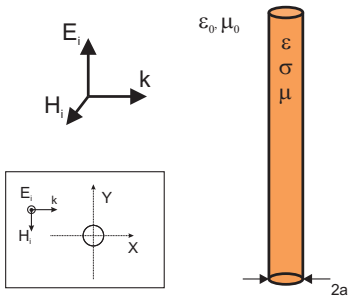

Fig. 1. Geometry of an infinitely long ferromagnetic wire excited by a uniform plane wave.

II. Infinitely-Long Wires: Theoretical Analysis

A. Absorption Spectrum from the Scattering Problem

The geometry of a ferromagnetic wire of radius a excited by a plane wave with its electric field polarized along the wire axis is schematically depicted in Fig. 1. For infinitely long wires, the problem is reduced to a 2D configuration as represented in the inset of the same figure.

In general, the power absorbed by the wire is rigorously found by integrating the Poynting vector on the surface of the wire:

$$P_{\text{abs}} = \frac{1}{2} \oiint_S \text{Re}\left[\mathbf{E} \times \mathbf{H}^*\right] \hat{\mathbf{n}} dS \tag{1}$$

where $\mathbf{E}$ and $\mathbf{H}$ are the electric and magnetic field on the wire surface, and $\hat{\mathbf{n}}$ is the unitary vector perpendicular to the surface of the wire. $\mathbf{E}$ and $\mathbf{H}$ can be found from previous studies on the scattering of ferromagnetic wires [12], [20], [21]. For conducting ferromagnetic wires, it has been theoretically found [7], [21] and experimentally verified (e.g. in resonant cavities [14] and rectangular waveguides [21]) that the response of the wire is dominated by the uniform electric current flowing along the wires. In this case, the fields in the wire have perfect azimuthal symmetry, and thus (1) simplifies to

$$P_{\text{abs}}^{L} = 2\pi a \cdot \frac{1}{2} \text{Re}\left[E_z H_\phi^*\right] \tag{2}$$

Note that since it is a 2D problem, the absorbed power, $P_{\rm abs}$, has been addressed as absorbed power per unit length, $P^L_{\rm abs}$. In general, E_z and H_ϕ are a complex function of the wire geometry, conductivity and magnetization state. In this work the expressions of E_z and H_ϕ uniform and static magnetizations introduced in [21] (equations (17) and (19) within the reference) and/or in [12] (equations (A8) and (A9)) will be employed, since it is the expected response for saturated wires. In other words, exchange interactions will be neglected in the rest of the paper.

Therefore, the wires are magnetically characterized by a permeability dyadic $\overline{\overline{\mu}} = \mu\overline{\overline{I}}_t + \mu_0\hat{\mathbf{z}}\hat{\mathbf{z}} - j\mu_t\hat{\mathbf{z}} \times \overline{\overline{I}}_t$, where μ and μ_t are the diagonal and off-diagonal permeability components with Lorentzian frequency behaviour. For the studied polarization, the wires response is equivalent to an effective permeability $\mu_e = \left(\mu^2 - \mu_t^2\right)/\mu$. Fig. 2a shows the effective permeability of a ferromagnetic wire around the FMR frequency. Typical parameters of Co-rich wires [13] have been adopted: gyromagnetic ratio $\gamma = 2 \cdot 10^{11}\ \mathrm{T^{-1}s^{-1}}$, saturation magnetization $\mu_o M_s = 0.55$ T, conductivity $\sigma = 5 \cdot 10^5\ \mathrm{S/m}$ and magnetic losses factor $\alpha = 0.02$. In addition, the effective DC magnetic field has been fixed to $H_{\rm eff} = 95\ \mathrm{kA/m}$ to center the FMR at 9 GHz. As it is shown, the effective permeability follows a Lorentzian resonant behaviour, with a maximum of magnetic losses at the FMR frequency. Furthermore, its real part is positive below the FMR frequency and negative above it.

In order to illustrate the complexity of the absorption spectrum, Fig. 2b depicts the absorption spectrum of wires with $22.5\,\mu$m, $5\,\mu$m and $2\,\mu$m radius. The magnitude of the incident electric field has been fixed to $E_0 = 1\ \mathrm{V/m}$, leading to an incident power density $\mathcal{P}_{\rm in} = 1/(2\eta)\ \mathrm{W/m^2}$. It can be concluded that the absorption spectrum is strongly correlated with the wire radius: Firstly, the absorption spectrum of the wire with $22.5\,\mu$m radius presents a maximum of absorption close to the FMR but at slightly higher frequencies. Secondly, the absorption spectrum of the wire with $5\,\mu$m is characterized by the sequence of a minimum and maximum, none of them centered at the FMR frequency. More strikingly, the absorption spectrum of the wire with $2\,\mu$m features minimal absorption at the FMR frequency. This complex behaviour reveals that the absorption is not necessarily enhanced by the FMR, which must be taken into account in the design of ferromagnetic wire-based devices. Moreover, the FMR cannot be easily identified from the absorption spectrum.

B. Equivalent Circuit Model

This complex response can be clarified with the aid of an equivalent circuit model. By defining the equivalent current $I = 2\pi a H_\phi$ and wire distributed impedance $Z_{\rm w} = E_z/I$, (2) can be rewritten in terms of circuital elements as follows

$$P^L_{\rm abs} = \frac{1}{2} R_{\rm w} |I|^2 \tag{3}$$

where $R_{\rm w} = \mathrm{Re}\left[Z_{\rm w}\right]$ stands for the real part of the wire distributed impedance, given by [7]

$$Z_{\rm w} = R_{\rm w} + jX_{\rm w} = \frac{j\eta_{\rm w}}{2\pi a} \cdot \frac{J_0\left(k_{\rm w} a\right)}{J_0'\left(k_{\rm w} a\right)} \tag{4}$$

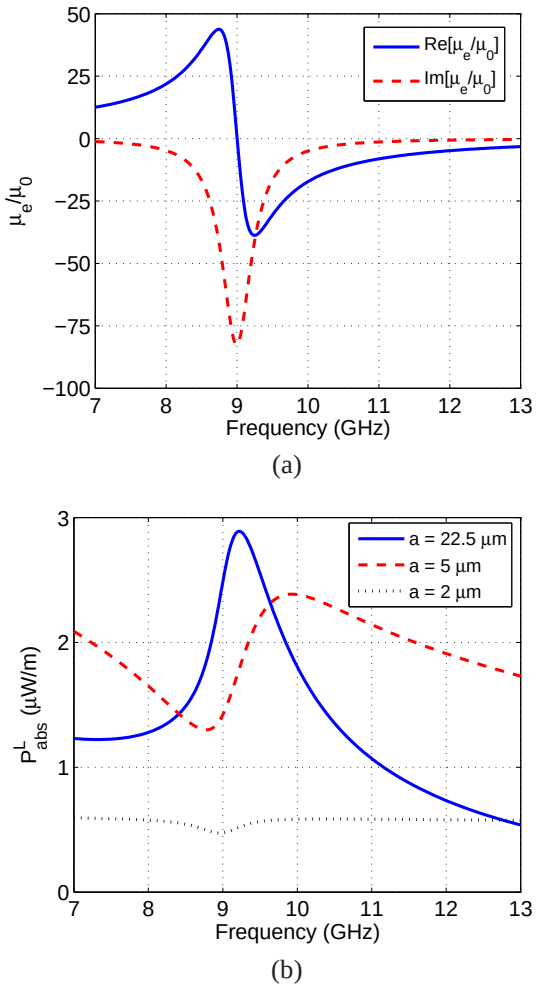

Fig. 2. (a) Effective relative permeability and (b) absorption spectrum for Co-rich wires with $22.5\,\mu$m, $5\,\mu$m and $2\,\mu$m radius.

where $\eta_{\rm w} = \sqrt{\mu_{\rm e}/\epsilon}$ and $k_{\rm w}^2 = \omega^2\mu_{\rm e}\epsilon$ stand for the medium impedance and propagation constant inside the wire, where the wire permittivity $\epsilon = -j\sigma/\omega$ is mostly controlled by the conductivity. $J_0(-)$ is the Bessel function of the first kind and zero-th order.

Reordering the terms of H_ϕ introduced in Refs. [21] and [12], the equivalent current I can also be rewritten in circuital terms as follows

$$I = \frac{E_0}{Z_{\rm w} + R_{\rm rad} + j\omega L_\sigma} \tag{5}$$

where $R_{\rm rad}$ takes into account the radiation losses of the wires, and can be written as

$$R_{\rm rad} = \frac{\eta k}{4} \tag{6}$$

where $\eta = \sqrt{\mu_0/\epsilon_0}$ and $k^2 = \omega^2\mu_0\epsilon_0$ stand for the medium impedance and propagation constant in free-space.

Moreover, L_σ takes into account the inductance produced by the equivalent current, and is given by

$$L_\sigma = \frac{\mu_0}{2\pi}\left[\ln\left(\frac{2}{ka}\right) + 0.5772\right] \tag{7}$$

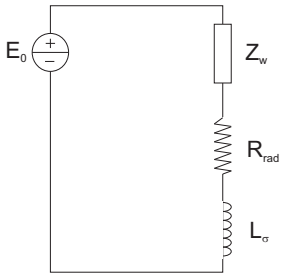

Fig. 3. Equivalent circuit model of the scattering and absorption of a long conductive ferromagnetic wire.

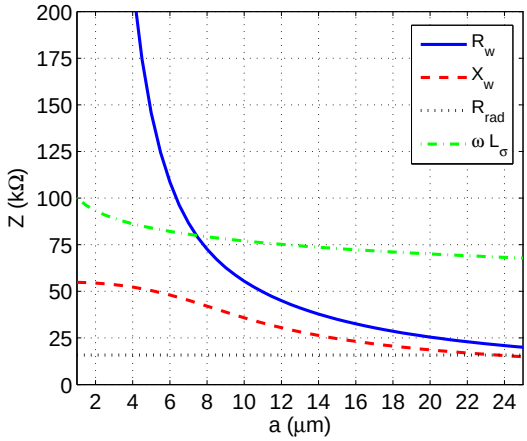

Fig. 4. Wire distributed impedance $Z_{\rm w} = R_{\rm w} + jX_{\rm w}$, radiation resistance $R_{\rm rad}$ and inductance produced by the equivalent current ωL_σ as a function of the wire radius. The frequency has been fixed at 8 GHz.

In summary, this circuit formulation reflects that the scattering problem is equivalent to the simple equivalent circuit represented on Fig. 3. Note that this circuit is not an approximation, but just a more intuitive way to rewrite the solution to the scattering problem.

In order to provide more physical insight into the equivalent circuit model, note that the importance of each of the impedance terms in (5) depends on the geometry of the wire. On the one hand, thick wires with strong skin-effect behave as good conductors, so that the inductance term L_σ is dominant. On the opposite extreme, the wire resistance $R_{\rm w}$ is dominant for very thin wires, in which the skin-effect is weak. This is evidenced in Fig. 4, which represents the wire distributed impedance, the radiation resistance and the inductance produced by the equivalent current as a function of the wire radius.

The results were obtained for a frequency of 8 GHz. As for the frequency dependence of such impedance contributions, the behavior of the wire distributed impedance, radiation resistance and inductance produced by the equivalent current for a wire of $22.5\ \mu$m radius are represented in Fig. 5. As it is shown, the wire distributed impedance follows the Lorentzian resonant behavior of the wire permeability, with maximum resistance at the FMR, and a reactance that is inductive below FMR and capacitive above it. In addition,

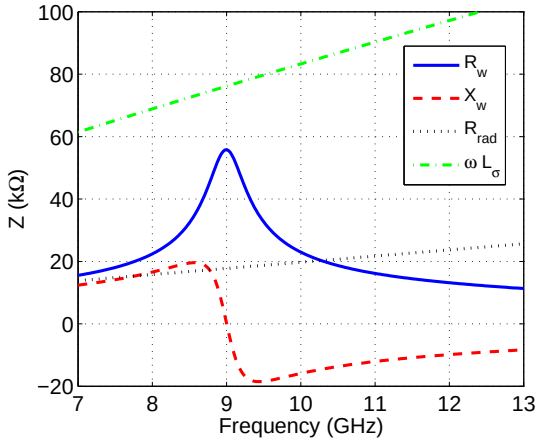

Fig. 5. Frequency-domain behavior of the real and imaginary parts of the wire distributed impedance, radiation resistance and inductance produced by the equivalent current. Wire radius of $22.5\ \mu$m.

the reactance produced by the equivalent current and radiation resistance naturally increase along with frequency.

C. Interpretation of the Absorption Spectra

The previous analysis provides an intuitive explanation for the absorption spectra depicted in Fig. 2. For thick wires, L_σ is dominant, so that the absorbed power simplifies to

$$P_{\rm abs}^{L} \simeq \frac{1}{2} R_{\rm w} \frac{E_0^2}{\left(\omega L_\sigma\right)^2} \tag{8}$$

Therefore, the absorption spectra is expected to show a maximum of absorption at the FMR, corresponding to the maximum of wire resistance, $R_{\rm w}$. In other words, if the inductance produced by the equivalent current, L_σ, is dominant, the wire distributed impedance, $Z_{\rm w}$, has no impact on the equivalent current, I, and the absorption is maximized at the maximum of losses.

Contrarily, $Z_{\rm w}$ affects I for smaller radii. This shifts the absorption maximum towards higher frequencies, since the capacitive contribution of $X_{\rm w}$ above the FMR compensates L_σ increasing I, which can be observed for the wire of $22.5\ \mu$m radius in Fig. 2. Similarly, the inductive contribution of $X_{\rm w}$ below the FMR produces a decrease of I, and thus a minimum of absorption. Therefore, the absorption spectra of wires with intermediate radii are characterized by the sequence of a minimum and a maximum, as it is observed for the wire of $5\ \mu$m radius in Fig. 2.

Finally, for very thin wires, the wire resistance $R_{\rm w}$ is dominant, so that the absorbed power simplifies to

$$P_{\rm abs}^{L} \simeq \frac{1}{2} R_{\rm w} \frac{E_0^2}{R_{\rm w}^2} = \frac{1}{2} \frac{E_0^2}{R_{\rm w}} \tag{9}$$

which explains the minimum of absorption at the FMR resonance observed for the wire of $2\ \mu$m radius in Fig. 2. In circuital terms, the excess of losses at the FMR produces a reduction of the excited current, which leads to a minimum of absorption.

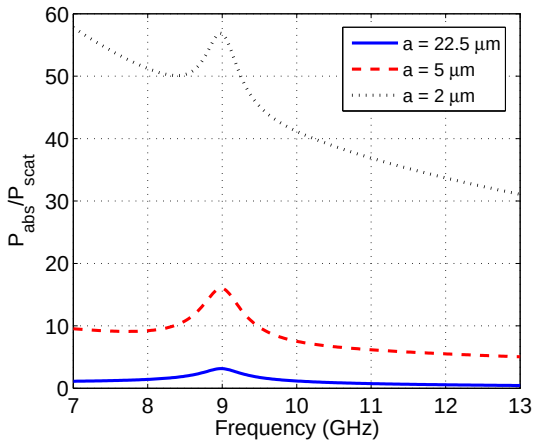

Fig. 6. Absorbed to scattered power ratio spectra for Co-rich wires with $22.5\,\mu$m, $5\,\mu$m and $2\,\mu$m radius.

Although this equivalent circuit model clarifies the absorption spectrum, it is still not possible to identify the exact position of the FMR. This can be solved by noting that the scattered power, $P^L_{\rm scat}$, is also proportional to the square of I

$$P^L_{\rm scat} = \frac{1}{2}\oiint_S \mathrm{Re}\left[\mathbf{E}^s \times \mathbf{H}^{s*}\right]\hat{\mathbf{n}}dS = \frac{1}{2}R_{\rm rad}\left|I\right|^2 \tag{10}$$

Thus, the absorbed to scattered power ratio defined here as

$$\frac{P_{\rm abs}}{P_{\rm scat}} = \frac{R_{\rm w}}{R_{\rm rad}} \tag{11}$$

is independent of the current excited in the wire, and features a maximum at the FMR independently on the wire geometry. Fig. 6 depicts the $P_{\rm abs}/P_{\rm scat}$ spectra for Co-rich wires with $22.5\,\mu$m, $5\,\mu$m and $2\,\mu$m radius. As expected, a maximum at 9 GHz is observed for all studied radii. In addition, $P_{\rm abs}/P_{\rm scat}$ increases as the radius decreases due to the increase in $R_{\rm w}$.

III. Infinitely-Long Wires: Experimental Verification

Three different $(Co_{0.94}Fe_{0.06})_{75}Si_{12.5}B_{12.5}$ ferromagnetic wires with $22.5\,\mu$m, $5\,\mu$m and $2\,\mu$m metallic radius and mean total diameter (including the Pyrex coating) of $65\,\mu$m, $33\,\mu$m and $14\,\mu$m, respectively, have been employed to experimentally validate the theoretical analysis. The samples have been fabricated by means of the Taylor-Ulitovsky technique at the Material Science Institute of Madrid (ICMM), Prof. M. Vázquez.

A sketch and photograph of the experimental setup are presented in Fig. 7. The wire is placed between two rectangular metallic WR-90 waveguides, so that when they are connected the wire is short-circuited and behaves as the theoretically studied infinitely long wires. The setup has been calibrated at the waveguide ends. Moreover, an electromagnet is employed to apply a DC magnetic field along the wire axis. The frequency range is selected so that monomode operation is

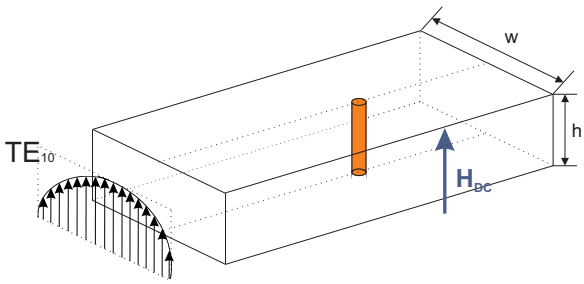

(a)

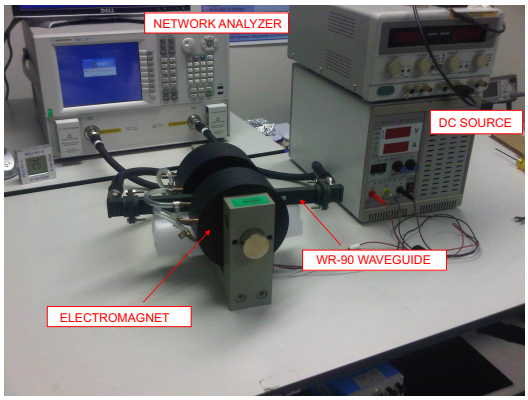

(b)

Fig. 7. (a) Sketch and (b) photograph of the experimental setup. The microwire is placed in the middle of a WR-90 waveguide with its ends short-circuited to the metallic walls. An electromagnet has been positioned in such way that a DC magnetic field is applied parallel to the microwire axis.

ensured, with the TE_{10} waveguide mode as incident high-frequency field. The reflection R, transmission T and absorption A power coefficients can be directly obtained from the measurement of the S-parameters: $R = |S_{11}|^2$, $T = |S_{21}|^2$ and $A = 1 - |S_{11}|^2 - |S_{21}|^2$.

Theoretical analysis of the experimental setup can be found in Refs. [21], [22]. In essence, the incident electromagnetic field impinges on the ferromagnetic wire, which scatters some electromagnetic power in the form of cylindrical waves that, due to the influence of the metallic walls, is reflected back and transmitted forward as the TE_{10} waveguide mode. Therefore, the scattered power is proportional to twice the measured reflection coefficient, $P_{\rm scat} \propto 2R$, and the absorbed power is proportional to the absorption coefficient, $P_{\rm abs} \propto A$. Consequently, the absorbed to scattered power ratio is estimated as $P_{\rm abs}/P_{\rm scat} \simeq A/2R$.

Fig. 8a represents the measured absorbed to scattered power ratio for the wire with $22.5\,\mu$m radius. Each line corresponds to a different biasing DC magnetic field as indicated in Table I. While the response is flat for a null biasing $H_1 = 0$ kA/m, the absorbed to scattered power ratio of biased wires is characterized by a peak that increases its frequency position along with H_{DC}. According to the theory, this peak identifies the FMR and has been marked with a vertical line to compare it with the absorption spectrum, which is represented in Fig. 8b. The absorption spectrum is also characterized by a peak that increases its frequency position along with H_{DC}. In accordance with the theoretical predictions, these absorption

TABLE I
H_{DC} BIASING MAGNETIC FIELD

H_1	0 kA/m
H_2	89.4 kA/m
H_3	117.7 kA/m
H_4	146.0 kA/m

maxima are shifted towards higher frequencies with respect to the FMR.

The measurements of the wire with $5\ \mu$m radius are depicted in Fig. 9. Again, the absorbed to scattered power ratio is characterized by a maximum peak, and the measured values are larger than those obtained for the wire of $22.5\ \mu$m radius. Despite using the same bias field and wire composition, the FMR frequencies do not coincide with those of the $22.5\ \mu$m radius wire. Note that this is a typical effect in glass-coated amorphous wires [23], produced by changes on the magnetic properties of the wires due to the mechanical stresses produced during the fabrication processes, which are a function of the wire geometry (metallic and total radius). As for the absorption spectrum, it describes a minimum-maximum sequence as predicted by the theory (see Fig. 9b).

Finally, the absorbed to scattered power ratio and absorption spectra of the wire with $2\ \mu$m radius are depicted in Figs. 10a and 10b, respectively. As with the other wires, the absorbed to scattered power ratio spectrum is characterized by a maximum, which confirms the independency of this figure with respect to the geometry. As expected, the measured values of absorbed to scattered power ratio increase with respect to the other wires. In addition, the absorption minima are centered at the FMR in accordance to the theoretical model.

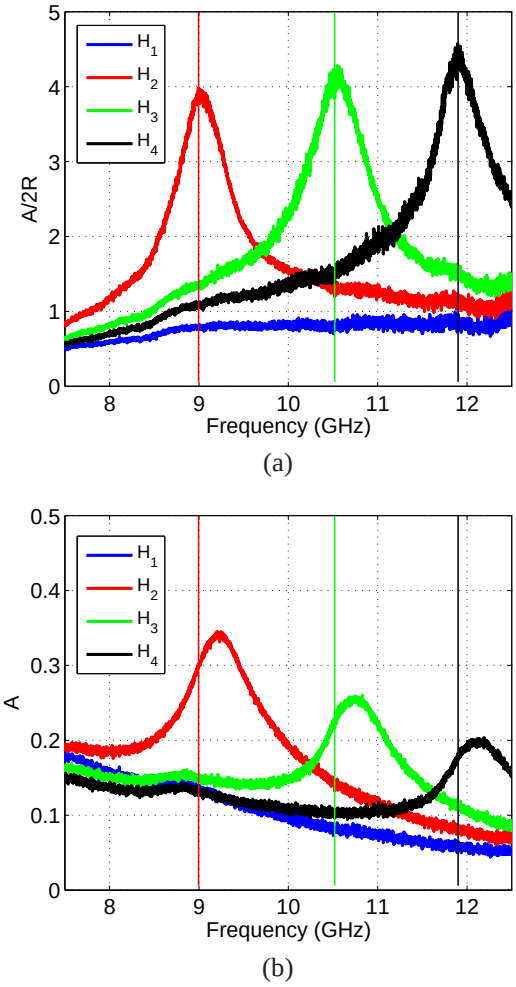

Fig. 8. [Color Online] Measured (a) absorbed to scattered power ratio and (b) absorption, for a Co-rich ferromagnetic wire of $a = 22.5\,\mu$m radius, as a function of the applied DC magnetic field.

IV. Finite-Length Wires: Theoretical Analysis

A. Absorption Spectrum from the Scattering Problem

Once the response of infinite-length wires has been explained, let us focus on the finite-length wires case. Consider the ferromagnetic wire of length $2L$ and radius a depicted in Fig. 11. In virtue of the Huygens Principle and equivalence theorem [24], the original problem can be transformed to an equivalent one by including electric and magnetic currents on the surface of the wire. Thus, the scattering problem ($\mathbf{E}^i(\mathbf{r}) + \mathbf{E}^s(\mathbf{r}) = \mathbf{E}(\mathbf{r})$, i.e. total field is equal to the addition of the incident and scattered fields) is reduced to the following integro-differential equation

$$E_0\hat{\mathbf{z}} - \frac{j}{\omega\varepsilon_0}\left[k^2 + \nabla\nabla\cdot\right]\iint_S \mathbf{J}_S(\mathbf{r}')\cdot\frac{e^{-jkR}}{4\pi R}dS - \nabla\times\iint_S \mathbf{M}_S(\mathbf{r}')\cdot\frac{e^{-jkR}}{4\pi R}dS = \mathbf{E}(\mathbf{r}) \tag{12}$$

where $\mathbf{J}_S$ and $\mathbf{M}_S$ are the equivalent electric and magnetic currents, respectively, which are given by

$$\mathbf{J}_S(\mathbf{r}') = \hat{\mathbf{n}}\times\mathbf{H} = H_\phi(z')\hat{\mathbf{z}} = \frac{I(z')}{2\pi a}\hat{\mathbf{z}} \tag{13}$$

$$\mathbf{M}_S(\mathbf{r}') = -\hat{\mathbf{n}}\times\mathbf{E} = E_z(z')\hat{\boldsymbol{\phi}} = Z_{\mathrm{w}}I(z')\hat{\boldsymbol{\phi}} \tag{14}$$

For the particular case of microwires $a \ll \lambda$ and $a \ll L$ are simultaneously fulfilled, and thus (12) is reduced to a generalized Pocklington equation

$$\frac{j\eta}{2\pi}\left[k^2 + \frac{\partial^2}{\partial z^2}\right]\int_{-L}^{L} I(z')\cdot G(R)\,dz' - 2kZ_{\mathrm{w}}I(z) = 2kE_0 \tag{15}$$

where $G(R)$ is the exact thin wire kernel equal to

$$G(R) = \int_0^{2\pi}\frac{e^{-jkR}}{4\pi R}d\phi' \tag{16}$$

with

$$R^2 = (z-z')^2 + r^2 - 2ra\cdot\cos(\phi') \tag{17}$$

The solution to this integro-differential equation provides the surface current, $I(z)$. Analytical solutions to this equation have been introduced in [25]–[27]. However, the equation has several solutions and an iterative process is in general needed to achieve the correct value. Despite this, it has been proven that simple numerical methods can be adopted leading to accurate solutions [28]. In this work, (15) is solved by using the method of moments following a point matching scheme with a triangular basis functions.

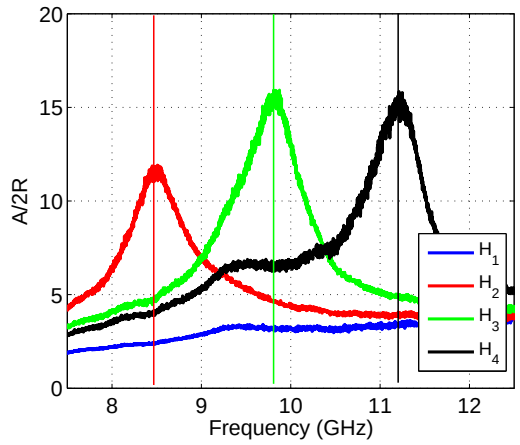

(a)

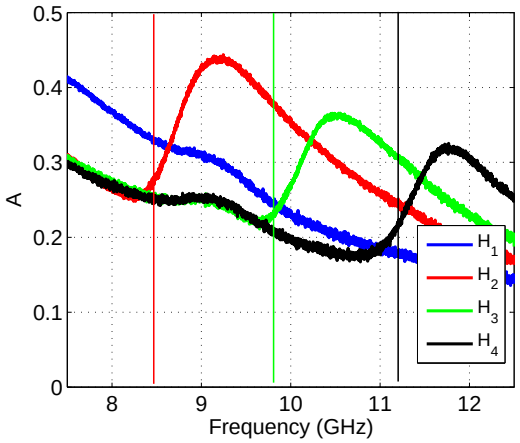

(b)

Fig. 9. [Color Online] Measured (a) absorbed to scattered power ratio and (b) absorption, for a Co-rich ferromagnetic wire of $a = 5\,\mu$m radius, as a function of the applied DC magnetic field.

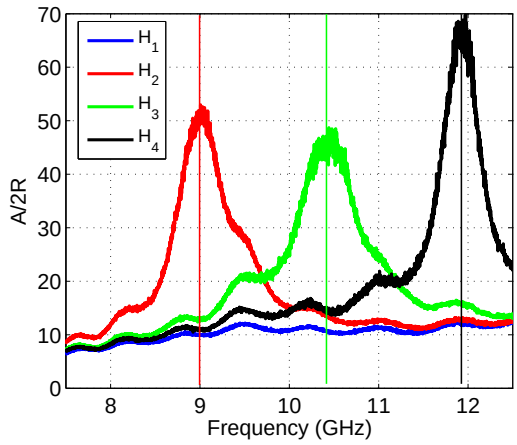

(a)

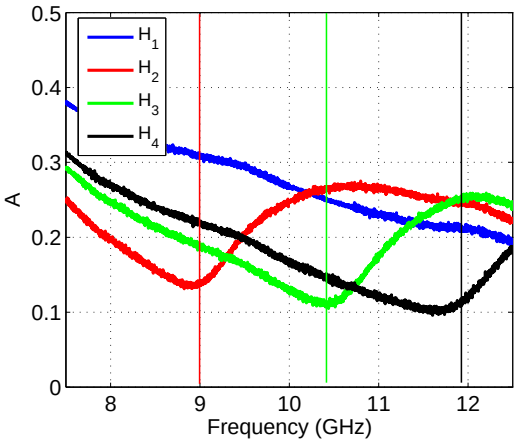

(b)

Fig. 10. [Color Online] Measured (a) absorbed to scattered power ratio and (b) absorption, for a Co-rich ferromagnetic wire of $a = 2\,\mu$m radius, as a function of the applied DC magnetic field.

Once the surface current $I(z)$ is known, the electric and magnetic fields on the surface of the wires can be easily retrieved, and thus compute the absorbed and scattered powers. Again, the absorbed power is determined by integrating the Poynting vector on the surface of the wire

$$\begin{aligned} P_{\rm abs} &= \frac{1}{2}\oiint_S Re\left[\mathbf{E}\times\mathbf{H}^*\right]\hat{\mathbf{n}}dS \\ &= \frac{1}{2}R_{\rm w}\int_{-L}^{L}|I(z)|^2\,dz \end{aligned} \tag{18}$$

Similarly, the scattered power is computed by integrating the Poynting vector of the scattered field on the surface of the wire

$$\begin{aligned} P_{\rm scat} &= \frac{1}{2}\oiint_S Re\left[\mathbf{E}^s\times\mathbf{H}^{s*}\right]\hat{\mathbf{n}}dS \\ &= \frac{1}{2}R_{\rm rad}\int_{-L}^{L}|I(z)|^2\,dz \end{aligned} \tag{19}$$

B. Approximate Circuit Model

While the previous analysis represents a complete solution to the scattering problem, it must be solved numerically and can hardly provide much physical insight into the absorption spectrum. Therefore, this section introduces a simple circuit model that, despite being an approximation of the scattering solution, it is reasonably accurate, and simple enough to provide physical insight into the correlation between the absorption spectrum and the geometry of the wire.

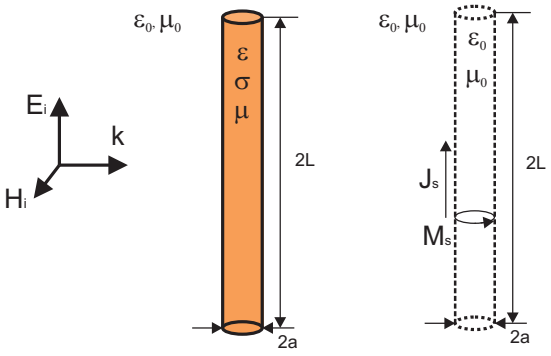

Fig. 11. Geometry of the original and equivalent problems of the scattering from a finite-length ferromagnetic wire.

To begin with, the solution to the scattering problem becomes easier if the current distribution on the wire is known. As with dipole antennas, the current can be approximated by sinusoidal distributions [29]. In particular, the current distribution of a receiving dipole antenna is given by

$$I(z) = I_R(0) \cdot f_R(z) \tag{20}$$

with

$$f_R(z) = \frac{\cos(kz) - \cos(kL)}{1 - \cos(kL)} \tag{21}$$

Thus, the problem is reduced to finding the magnitude of the current, $I_R(0)$. Furthermore, $I_R(0)$ can be easily determined by means of the reciprocity theorem as follows [30]

$$I_R(0) = \frac{V}{Z_{\text{in}} + Z_{\text{w}}^{\text{mod}}} \tag{22}$$

where V stands for the induced electromotive force, given by

$$V = E_0 \int_{-L}^{L} f_T(z)\, dz \tag{23}$$

with $f_T(z)$ being the current distribution function of the reciprocal antenna in the transmitting mode

$$f_T(z) = \frac{\sin(kL - k|z|)}{\sin(kL)} \tag{24}$$

In addition, Z_{in} is the self-impedance of the reciprocal transmitting antenna, and $Z_{\text{w}}^{\text{mod}}$ is an impedance term which takes into account the wire surface impedance, Z_{w}. In particular, the finite conductivity and magnetic response of the wire produce a voltage drop $Z_{\text{w}} f_T(z)$ at each dz point of the wire, which is modeled as an additional impedance term $Z_{\text{w}}^{\text{mod}}$, defined as

$$Z_{\text{w}}^{\text{mod}} = Z_{\text{w}} \int_{-L}^{L} f_T^2(z)\, dz \tag{25}$$

Once the current on the wire has been determined through the circuit model, the absorbed and scattered powers can again be computed through (18) and (19).

The accuracy of this circuit model basically relies on the validity of the sinusoidal currents assumption. Therefore, the circuit model will be accurate as long as the wires behave as good conductors (i.e. thick wires). Fig. 12 depicts the comparison of the absorption spectra predicted by the method of moments and the circuit model for Co-rich wires with $22.5\,\mu\text{m}$, $5\,\mu\text{m}$ and $2\,\mu\text{m}$ radius and $2L = 9.8\,\text{mm}$ length. While there is almost a perfect match between both models for the thickest wire, the accuracy of the circuit model degrades as the wire radius decreases. Nevertheless, the circuit model provides a qualitative estimation of the absorption spectrum for all considered radii.

As for the absorbed to scattered power ratio, (18) and (19) show that $P_{\text{abs}}/P_{\text{scat}} = R_{\text{w}}/R_{\text{rad}}$ is again independent of the current induced in the wire and thus both methods retrieve exactly the same result, which is in fact equal to the ratio obtained for infinitely-long wires.

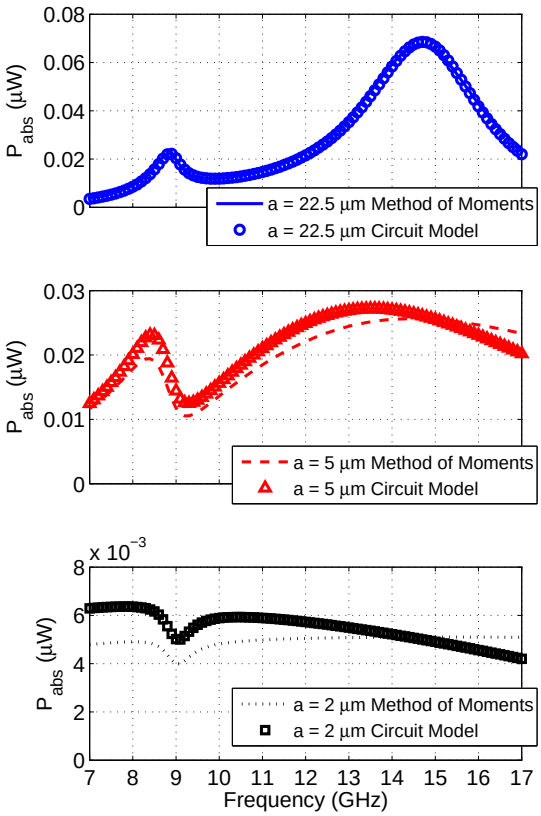

Fig. 12. Comparison of the absorption spectrum predicted by the method of moments and circuit model for Co-rich wires with $22.5\,\mu\text{m}$, $5\,\mu\text{m}$ and $2\,\mu\text{m}$ radius and $2L = 9.8\,\text{mm}$ length.

C. Interpretation of the Absorption Spectrum

Fig. 12 also reveals the main features of the absorption spectrum for finite length wires. To further clarify this spectrum, Fig. 13 represents the modified wire surface impedance $Z_{\text{w}}^{\text{mod}} = R_{\text{w}}^{\text{mod}} + jX_{\text{w}}^{\text{mod}}$ of a wire with $2L = 9.8\,\text{mm}$ length and $a = 22.5\ \mu\text{m}$ radius, as well as the input impedance of the reciprocal transmitting antenna, $Z_{\text{in}} = R_{\text{in}} + jX_{\text{in}}$. While $Z_{\text{w}}^{\text{mod}}$ has been evaluated through (25), Z_{in} has been calculated as in basic antenna textbooks (see e.g. [29], p. 918). The figure shows that $Z_{\text{w}}^{\text{mod}}$ is a scaled version of Z_{w} (see Fig. 5), while Z_{in} follows the typical behavior of a dipole antenna, with a resistance of approximately $75\ \Omega$ at 15.3 GHz ($L \simeq 0.5\lambda$), and zero reactance at approximately 14.9 GHz ($L \simeq 0.485\lambda$).

In view of the frequency dependence of these impedance terms, the two absorption peaks observed for the wire of $22.5\mu\text{m}$ radius (see Fig. 12) can be explained as follows: the first peak is centered close to 9 GHz, and therefore it is ascribed to the increase of losses at the FMR. On the contrary, the second peak is placed close to the half-wave antenna resonance, and thus it is produced by an increase of the current excited in the wire at $X_{\text{in}} = 0$.

As the wire radius decreases the wire resistance increases, which weakens the axial resonance. In fact, the second absorp-

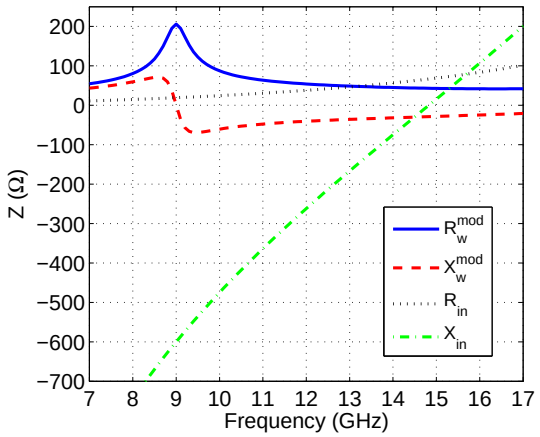

Fig. 13. Modified wire surface impedance $Z_{\rm w}^{\rm mod} = R_{\rm w}^{\rm mod} + jX_{\rm w}^{\rm mod}$ of a wire with $2L = 9.8\,\mathrm{mm}$ length and $a = 22.5\ \mu\mathrm{m}$ radius, as well as the input impedance of the reciprocal transmitting antenna, $Z_{\rm in} = R_{\rm in} + jX_{\rm in}$.

tion maximum diminishes from $0.07\ \mu\mathrm{W}$ for $22.5\ \mu\mathrm{m}$ radius to $0.025\ \mu\mathrm{W}$ for $5\ \mu\mathrm{m}$ radius, and it completely vanishes for the wire of $2\ \mu\mathrm{m}$ radius.

Note also that the maxima due to the FMR observed in the wires of $22.5\,\mu\mathrm{m}$ and $5\,\mu\mathrm{m}$ radius are located at lower frequencies than the FMR (below 9 GHz), while the absorption peaks of infinitely-long wire where observed at higher frequencies. This is justified by the capacitive $Z_{\rm in}$ at the FMR frequency (see. Fig. 13), in contrast to the dominant inductance of infinitely-long wires. As for the wire of $2\,\mu\mathrm{m}$ radius, the wire resistance is again dominant and a minimum of absorption is centered at the FMR.

D. Impact of the Pyrex Coating

Up to this point, the impact of the Pyrex coating on the wire response has been neglected. In fact, the same assumption is implicit in previous theoretical studies on the electromagnetic response of the wires both for infinitely-long [7], [20] and finite-length [9] wires. This assumption is based on the weak dielectric response of Pyrex ($\epsilon_p \simeq 4.9$) as compared to the ferromagnetic core. Additionally, this dielectric coating is placed in a minimum of electric field for wires behaving as good conductors.

Nevertheless, the Pyrex coating might perturb the axial resonances excited in finite-length wires, and thus significantly affect the absorption spectra. To include the coating in this study, the scattering problem addressed in Refs. [7], [12], [20] must be completed with an additional cylindrical region. As with other cylindrical layered structures [31], the result is a new wire with radius $a_{\rm c} = a + t$, where t is the thickness of the coating, and with a new distributed impedance, $Z_{\rm w}^{\rm c}$, given by

$$Z_{\rm w}^{\rm c} = \frac{j\eta_{\rm c}}{2\pi a_{\rm c}} \cdot \frac{J_0\left(k_{\rm c}a_{\rm c}\right) + T_1 \cdot H_0^{(2)}\left(k_{\rm c}a_{\rm c}\right)}{J_0'\left(k_{\rm c}a_{\rm c}\right) + T_1 \cdot H_0^{\prime(2)}\left(k_{\rm c}a_{\rm c}\right)} \tag{26}$$

with

$$T_1 = \frac{Z_{\rm w}J_0'\left(k_{\rm c}a\right) - \frac{j\eta_{\rm c}}{2\pi a}J_0\left(k_{\rm c}a\right)}{\frac{j\eta_{\rm c}}{2\pi a}H_0^{(2)}\left(k_{\rm c}a\right) - Z_{\rm w}H_0^{\prime(2)}\left(k_{\rm c}a\right)} \tag{27}$$

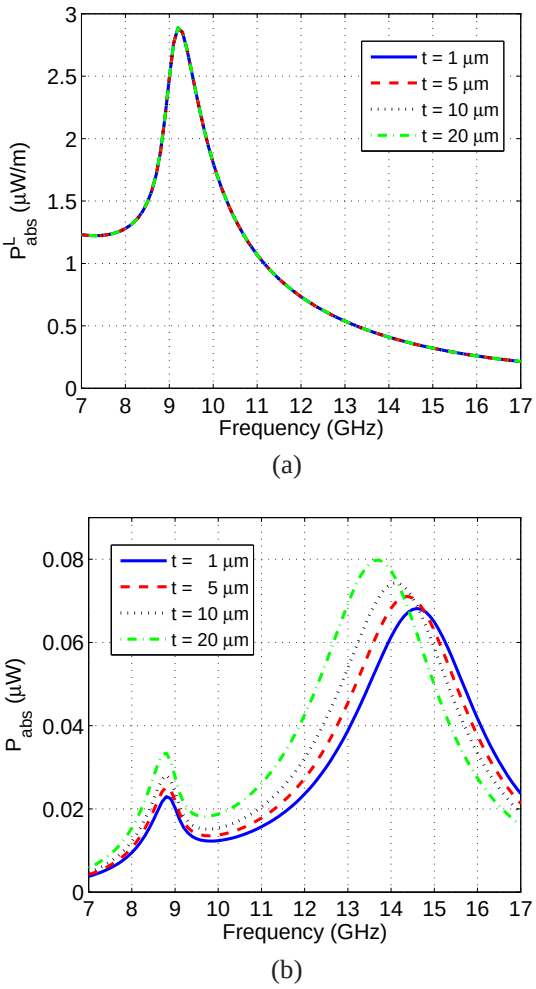

Fig. 14. Absorption spectrum of (a) an infinitely-long and (b) a $2L = 9.8\ \mathrm{mm}$ long Co-rich ferromagnetic wire of $a = 22.5\,\mu\mathrm{m}$ radius, and covered by with different Pyrex coatings of thickness $1\ \mu\mathrm{m}$, $5\ \mu\mathrm{m}$, $10\ \mu\mathrm{m}$ and $20\ \mu\mathrm{m}$

where $\eta_{\rm c}$ and $k_{\rm c}$ stand for the medium impedance and propagation constant inside the coating, and $Z_{\rm w}$ is the original wire distributed impedance, given by (4).

Fig. 14 represents the absorption spectrum of both, an infinitely-long, and a $2L = 9.8\ \mathrm{mm}$ long ferromagnetic wire of $a = 22.5\ \mu\mathrm{m}$ radius, covered by different Pyrex coatings of thickness $1\ \mu\mathrm{m}$, $5\ \mu\mathrm{m}$, $10\ \mu\mathrm{m}$ and $20\ \mu\mathrm{m}$. It can be concluded that the Pyrex coating has a negligible impact on the absorption spectrum of infinitely-long ferromagnetic wires, while it appreciably affects the spectrum of finite-length wires. The reason is again the alteration of the axial resonances in finite-length wires. In analogy to dipole antennas, covering the wire with a dielectric material increases its electrical size on the axial direction, and thus the axial resonances appear at lower frequencies.

V. Finite-Length Wires: Experimental Verification

The same $(\mathrm{Co}_{0.94}\mathrm{Fe}_{0.06})_{75}\mathrm{Si}_{12.5}\mathrm{B}_{12.5}$ ferromagnetic wires with $22.5\,\mu\mathrm{m}$, $5\,\mu\mathrm{m}$ and $2\,\mu\mathrm{m}$ metallic radius have been employed for the validation of theoretical results on finite-length wires. The experimental setup is also the one depicted

in Fig. 7, with the only difference that rather than connecting the wires to the waveguide walls, they have been cut to a length of 9.8 mm, and suspended within the waveguide on a Rohacell foam ($\epsilon_r \simeq 1.003$), with no contact with the metallic walls.

The spectra of absorbed to scattered power ratio and absorption for the wire of $22.5\,\mu\mathrm{m}$ radius are presented in Fig. 15. As it is shown, the unbiased wire ($H_1 = 0$) presents a flat spectrum of absorbed to scattered power ratio while its absorption spectrum is characterized by a maxima, not present in the infinitely-long wire (see Fig. 8). Therefore, this maximum is ascribed to an axial resonance in the wire.

For biased wires, a peak of absorbed to scattered power ratio can be observed in Fig. 15a, which again identifies the FMR. Moreover, an additional maximum appears on the absorption spectrum. As predicted by the theory, this maximum is produced by an increase of R_w at the FMR, but is located at lower frequencies due to the compensation of the capacitive input impedance ($X_\mathrm{in} < 0$), with the inductive $X_\mathrm{w} > 0$ below the resonance.

It is also observed that this frequency shift between the first absorption maxima and the FMR frequency increases along with the bias field. The reason is that the FMR frequency increases along with the bias field, so that a smaller X_in is placed at the FMR. Thus, the compensation of X_in with X_w gets stronger as compared to R_w, and therefore the shift of the absorption peak relative to the FMR increases along with the biasing field.

Note also that changing the biasing shifts towards higher frequencies the peak produced by the axial resonance, initially positioned at $X_\mathrm{in} = 0$. This is is produced by the $X_\mathrm{w} < 0$ above the FMR, so that $X_\mathrm{in} + X_\mathrm{w} = 0$ at higher frequencies. In addition, the closer the FMR and axial resonances are the larger is the magnitude of X_w, and the axial resonance is shifted towards higher frequencies.

A similar response is observed for the wire of $5\,\mu\mathrm{m}$ radius (see Fig. 16). The more remarkable difference is that as the electromagnetic fields penetrate more in the wire the axial resonance weakens, and the strength of both absorption peaks is comparable. In the same way, the shifts produced by the changes in the biasing fields are more pronounced.

On the contrary, a complete different response is observed for the wire of $2\,\mu\mathrm{m}$ radius. As anticipated in the theoretical analysis, Fig. 17b demonstrates that the axial resonance vanishes for very thin wires. In addition, a minimum of absorption appears at the FMR frequency. Unfortunately, the measurements of absorption to scattered power ratio were too noisy and cannot be interpreted (see Fig. 17a). The reason is the small reflection produced by a short wire of $2\,\mu\mathrm{m}$ radius ($6.67 \cdot 10^{-5}\lambda$ at 10 GHz).

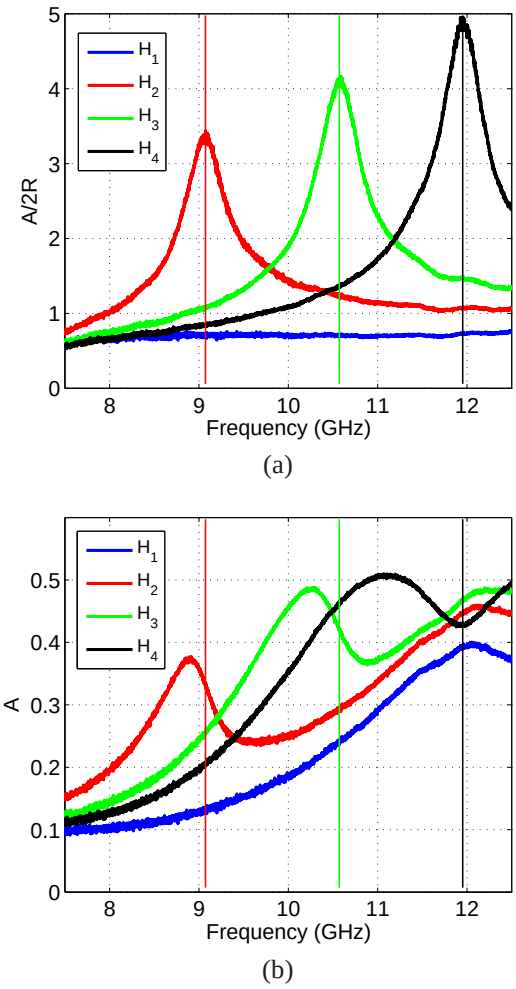

Fig. 15. [Color Online] Measured (a) absorbed to scattered power ratio and (b) absorption, for a Co-rich ferromagnetic wire of $a = 22.5\,\mu\mathrm{m}$ radius and $2L = 9.8\,\mathrm{mm}$ length, as a function of the applied DC magnetic field.

VI. Conclusions

A detailed analysis of the absorption spectrum of conductive ferromagnetic wires has been presented. The analysis involves the computation of the absorption spectrum from the solution to the scattering problem, the formulation of circuit models and the experimental validation of the theoretical results.

This analysis confirms the strong correlation between the absorption spectrum and the wire geometry. Therefore, the interpretation of the absorption spectrum is not straightforward, the FMR does not necessarily enhance the absorption and the FMR frequency cannot be localized. However, the absorption spectrum can be intuitively explained through circuit models and the FMR can be identified through the absorbed to scattered power ratio spectrum.

Furthermore, axial resonances are excited in finite-length wires as long as they are thick enough to behave as good conductors. This leads to additional absorption maxima in the proximity of half-wavelength resonances. In addition, there is an inter-coupling between axial and ferromagnetic resonances, which further alters the absorption spectra. On the contrary, the finite-length of the wires has no impact on the absorbed to scattered power ratio.

Acknowledgment

This work was supported by the Spanish Ministry of Science and Innovation, Dirección General de Investigación y Gestión del Plan Nacional de I+D+I, Subdirección General

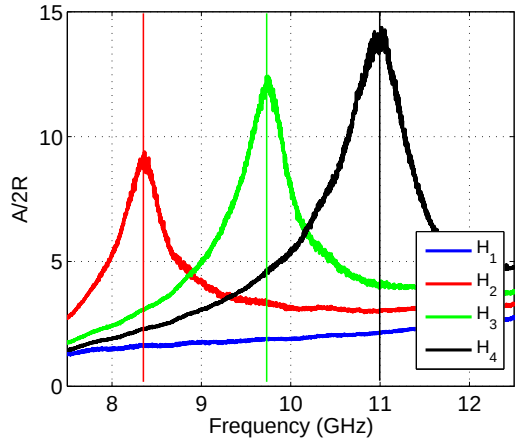

(a)

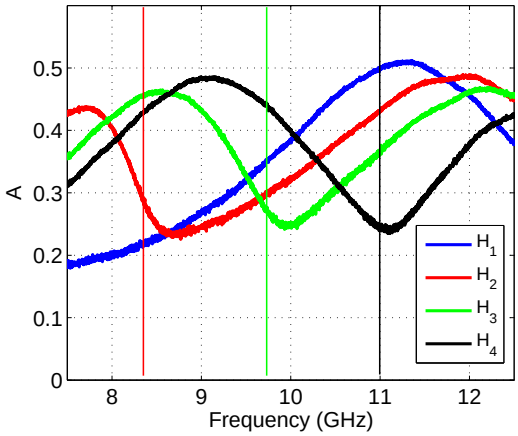

(b)

Fig. 16. [Color Online] Measured (a) absorbed to scattered power ratio and (b) absorption, for a Co-rich ferromagnetic wire of $a = 5\,\mu\mathrm{m}$ radius and $2L = 9.8\,\mathrm{mm}$ length, as a function of the applied DC magnetic field.

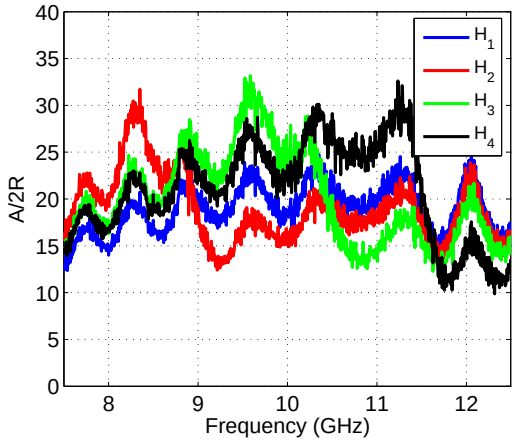

(a)

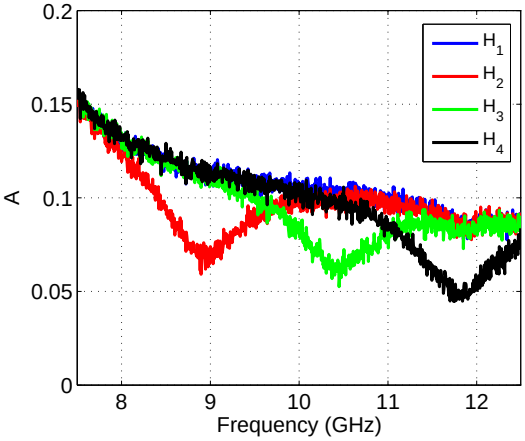

(b)

Fig. 17. [Color Online] Measured (a) absorbed to scattered power ratio and (b) absorption, for a Co-rich ferromagnetic wire of $a = 2\,\mu\mathrm{m}$ radius and $2L = 9.8\,\mathrm{mm}$ length, as a function of the applied DC magnetic field.

de Proyectos de Investigación, Project Nos. TEC2009-11995 and CSD2008-00066.

The authors thank Prof. M. Vázquez of the Material Science Institute of Madrid (ICMM) for providing the ferromagnetic wires.

REFERENCES

[1] S. A. Baranov, "Use of a microconductor with natural ferromagnetic resonance for radio-absorbing materials," *Technical Physics Letters*, vol. 24, no. 7, pp. 549–550, Jul. 1998.

[2] P. Marin, D. Cortina, and A. Hernando, "Electromagnetic Wave Absorbing Material Based on Magnetic Microwires," *IEEE Transactions on Magnetics*, vol. 44, no. 11, pp. 3934–3937, Nov. 2008.

[3] Z. Zhang, C. Wang, Y. Zhang, and J. Xie, "Microwave absorbing properties of composites filled with glass-coated Fe69Co10Si8B13 amorphous microwire," *Materials Science and Engineering: B*, vol. 175, no. 3, pp. 233–237, Dec. 2010.

[4] D. P. Makhnovskiy and L. V. Panina, "Experimental demonstration of tunable scattering spectra at microwave frequencies in composite media containing CoFeCrSiB glass-coated amorphous ferromagnetic wires and comparison with theory," *Physical Review B*, vol. 74, no. 6, pp. 1–11, Aug. 2006.

[5] F. X. Qin, N. Pankratov, H. X. Peng, M. H. Phan, L. V. Panina, M. Ipatov, V. Zhukova, A. Zhukov, and J. Gonzalez, "Novel magnetic microwires-embedded composites for structural health monitoring applications," *Journal of Applied Physics*, vol. 107, no. 9, p. 09A314, 2010.

[6] S. Starostenko and K. N. Rozanov, "Microwave Screen with Magnetically Controlled Attenuation," *Progress in Electromagnetic Research*, vol. 99, pp. 405–426, 2009.

[7] I. Liberal, I. S. Nefedov, I. Ederra, R. Gonzalo, and S. A. Tretyakov, "Electromagnetic response and homogenization of grids of ferromagnetic microwires," *Journal of Applied Physics*, vol. 110, no. 6, p. 064909, 2011.

[8] ——, "On the effective permittivity of arrays of ferromagnetic wires," *Journal of Applied Physics*, vol. 110, no. 10, p. 104902, 2011.

[9] D. P. Makhnovskiy and L. V. Panina, "Field dependent permittivity of composite materials containing ferromagnetic wires," *Journal of Applied Physics*, vol. 93, no. 7, p. 4120, 2003.

[10] L. V. Panina, M. Ipatov, V. Zhukova, A. Zhukov, and J. Gonzalez, "Magnetic field effects in artificial dielectrics with arrays of magnetic wires at microwaves," *Journal of Applied Physics*, vol. 109, no. 5, p. 053901, 2011.

[11] O. Reynet, A. Adenot-Engelvin, S. Deprot, O. Acher, and M. Latrach, "Effect of the magnetic properties of the inclusions on the high-frequency dielectric response of diluted composites," *Physical Review B*, vol. 66, no. 9, pp. 1–9, Sep. 2002.

[12] V. Boucher and D. Ménard, "Effective magnetic properties of arrays of interacting ferromagnetic wires exhibiting gyromagnetic anisotropy and retardation effects," *Physical Review B*, vol. 81, no. 17, pp. 1–21, May 2010.

[13] S. E. Lofland, H. García-Miquel, M. Vázquez, and S. Bhagat, "Microwave magnetoabsorption in glass-coated amorphous microwires with radii close to skin depth," *Journal of Applied Physics*, vol. 92, no. 4, p. 2058, 2002.

[14] L. Kraus, G. Infante, Z. Frait, and M. Vázquez, "Ferromagnetic reso-

nance in microwires and nanowires," *Physical Review B*, vol. 83, no. 17, pp. 4438–4449, May 2011.
[15] F. Yildiz, B. Z. Rameev, S. I. Tarapov, L. R. Tagirov, and B. Aktas, "High-frequency magnetoresonance absorption in amorphous magnetic microwires," *Journal of Magnetism and Magnetic Materials*, vol. 247, no. 2, pp. 222–229, Jun. 2002.
[16] G. Goglio, S. Pignard, A. Radulescu, L. Piraux, I. Huynen, D. Vanhoenacker, and A. V. Vorst, "Microwave properties of metallic nanowires," *Applied Physics Letters*, vol. 75, no. 12, pp. 1769 – 1772, 1999.
[17] H. García-Miquel, M. Esbri, J. Andres, J. Garcia, J. Garcia-Beneytez, and M. Vázquez, "Power absorption and ferromagnetic resonance in Co-rich metallic glasses," *IEEE Transactions on Magnetics*, vol. 37, no. 1, pp. 561–564, 2001.
[18] N.-E. Belhadj-Tahar, A. Fourrier-Lamer, and H. de Chanterac, "Broadband simultaneous measurement of complex permittivity and permeability using a coaxial discontinuity," *IEEE Transactions on Microwave Theory and Techniques*, vol. 38, no. 1, pp. 1–7, 1990.
[19] J. Garcia-Beneytez, F. Vinai, L. Brunetti, H. García-Miquel, and M. Vázquez, "Study of magneto impedance effect in the microwave frequency range for soft magnetic wires and microwires," *Sensors and Actuators A: Physical*, vol. 81, no. 1-3, pp. 78–81, Apr. 2000.
[20] L. Kraus, "Theory of ferromagnetic resonances in thin wires," *Czechoslovak Journal of Physics*, vol. 32, no. 11, pp. 1264–1282, Nov. 1982.
[21] I. Liberal, I. Ederra, C. Gomez-Polo, A. Labrador, J. Pérez-Landazabal, and R. Gonzalo, "Theoretical Modeling and Experimental Verification of the Scattering From a Ferromagnetic Microwire," *IEEE Transactions on Microwave Theory and Techniques*, vol. 59, no. 3, pp. 517–526, 2011.
[22] N. Okamoto, I. Nishioka, and Y. Nakanishi, "Scattering by a Ferrimagnetic Circular Cylinder in a Rectangular Waveguide," *IEEE Transactions on Microwave Theory and Techniques*, vol. 19, no. 6, pp. 521–527, 1971.
[23] A. Zhukov, M. Vázquez, J. Velázquez, A. Hernando, and V. Larin, "Magnetic properties of fe-based glass-coated microwires," *Journal of Magnetism and Magnetic Materials*, vol. 170, no. 3, pp. 323 – 330, 1997.
[24] C. A. Balanis, *Advanced Engineering Electromagnetics*. New York: Wiley, 1989.
[25] P. C. Waterman and J. C. Pedersen, "Scattering by finite wires," *Journal of Applied Physics*, vol. 72, no. 2, pp. 349–359, 1992.
[26] ——, "Scattering by finite wires of arbitrary ϵ, μ, and σ," *Journal of the Optical Society of America A*, vol. 15, no. 1, p. 174, 1998.
[27] P. C. Waterman, "Scattering, absorption, and extiction by thin fibers," *Journal of the Optical Society of America*, vol. 22, no. 11, pp. 2430–2441, 2005.
[28] S. Alyones, C. W. Bruce, and A. K. Buin, "Numerical Methods for Solving the Problem of Electromagnetic Scattering by a Thin Finite Conducting Wire," *IEEE Transactions on Antennas and Propagation*, vol. 55, no. 6, pp. 1856–1861, Jun. 2007.
[29] S. J. Orfanidis, *Electromagnetic Waves and Antennas*. Electronic Book: http://www.ece.rutgers.edu/ orfanidi/ewa/, 2008.
[30] S. A. Tretyakov, S. Maslovski, and P. A. Belov, "An analytical model of metamaterials based on loaded wire dipoles," *IEEE Transactions on Antennas and Propagations*, vol. 51, no. 10, pp. 2652–2658, Oct. 2003.
[31] B. J. Hu, E. K.-N. Yung, and X. Q. Sheng, "Electromagnetic scattering from nonuniform magnetized ferrite cylinder," *Microwave and Optical Technology Letters*, vol. 32, no. 4, p. 268 ? 272, 2002.

Iñigo Liberal was born on October 31, 1985 in Pamplona, Navarra, Spain. In 2009 he received the M. Sc. Degree in Telecommunication Engineering from the Public University of Navarra (UPNA), Pamplona, Spain. He was the recipient of a scholarship to carry out his M. Sc. Thesis at the International Research Center for Telecommunications and Radar (IRCTR) at the Delft University of Technology, The Netherlands.

Since August 2009 he has been with the Antenna Group at the Public University of Navarra (UPNA), where he is currently working towards his Ph.D. His main research interests are in the field of high-frequency applications of magnetic materials, the design of low-profile metamaterial-inspired antennas and UWB antenna systems.

Iñigo Ederra was born in Isaba, Navarra, Spain in 1972. He received the Ingeniero de Telecomunicación and Ph.D. degrees from the Universidad Pública de Navarra, Pamplona, Spain, in 1996 and 2004, respectively.

In 1997, he joined the Microwave and Millimetre Wave Group, Universidad Pública de Navarra. From 1999 to 2000 he was with the European Space Research and Technology Centre (ESTEC), ESA, Noordwijk, The Netherlands, where he was working on Electromagnetic Bandgap materials and their applications in the field of antennas. Since 2001 he is with the Antenna Group, Universidad Pública de Navarra. From June to October 2002 he was visitor scientist at the Rutherford Appleton Laboratory, Chilton, Didcot, UK, participating in the Startiger project.

He was co-recipient of the LAPC 2006 and IWAT 2007 best paper award. His research interests are in the field of Electromagnetic Bandgap materials and Metamaterials and their applications in microwave and millimetre wave components and antennas.

Cristina Gómez-Polo was born in Madrid, Spain. She received the M.Sc. and the Ph.D. degrees in Physics (Material Science) from the Complutense Universtity, Madrid, Spain, in 1988 and 1992, respectively. In 1995 she joined the Public University of Navarra as lecturer.

Her research activity is mainly focused on the magnetic properties and applications of nanostructured magnetic materials and include the study of amorphous, nanocrystalline and nanoparticle systems.

Alberto Labrador was born in Pamplona, Navarra, Spain on June 4, 1981. He received the M.Sc. degree in telecommunication engineering from Public University of Navarra (UPNA), Pamplona, Spain, in 2008.

Since December 2008 until July 2010, he was working at Public University of Navarra (UPNA) in Physics Department in Physical properties and applications of materials Group. His research was focused on the analysis of ferromagnetic microwires properties and the applications of these microwires in metamaterials development. To carry out this research he received a scholarship from Gobierno de Navarra.

Jose Ignacio Pérez-Landazábal received the Ph.D. degree in solid state physics in 1995 from Bask Country University in Spain. He is currently Associate Professor in the Physics Department of the Public University of Navarra.

His current research interests include Ferromagnetic Shape Memory alloys and magnetic properties of nanoparticles. He is interested in all experimental aspects related to phase transformations and its influence on their magnetic and themo-mechanical properties of materials.

Ramón Gonzalo (S 95) was born on July 15, 1972 in Logroõ, La Rioja. He received the M.Sc. and the Ph. D. degree in Ingeniero de Telecomunicación both with honors, from the Public University of Navarra (UPNa), Spain.

Since October 1995 he is with the Antennas Group at the Electrical and Electronic Engineering Department in UPNa where he currently is Associate Professor. From September 1997 to December 1998, he was joined as Research Fellow to the Antenna Section in ESA-ESTEC where he was involved in the modelling and design of electromagnetic crystal devices at microwave and millimetre wave frequencies. He has been involved in more than 25 research project, European, and National level acting as co-ordinator in several of them. In particular he has been co-ordinator of 5 projects funded by the European Space Agency, 2 projects in the framework of the European Commission and several of them funded by the Spanish Minister of Science. He has more than 50 journal publications in peer review magazines and 100 conference papers related to his research lines. From January 2006 untill April 2008 he was acting as sub-director of the Engineering Faculty and from April 2008 he is acting as Head of Electrical and Electronic Engineering Department.

His current area of research is in the field of Terahertz technologies, sub-systems and devices, Electromagnetic Band Gap technology with emphasis on space antenna applications, design of waveguide transmission lines and corrugated horn antennas.